Realization of a Distributed Bragg Reflector for Propagating Guided Matter Waves

C. M. Fabre, P. Cheiney, G. L. Gattobigio, F. Vermersch, S. Faure, R. Mathevet, T. Lahaye, and D. Guéry-Odelin

Université de Toulouse, UPS, Laboratoire Collisions Agrégats Réactivité, IRSAMC, F-31062 Toulouse, France and CNRS, UMR 5589, F-31062 Toulouse, France

(Received 27 July 2011; published 29 November 2011)

We report on the experimental study of a Bragg reflector for guided, propagating Bose-Einstein condensates. A one-dimensional attractive optical lattice of finite length created by red-detuned laser beams selectively reflects some velocity components of the incident matter wave packet. We find quantitative agreement between the experimental data and one-dimensional numerical simulations and show that the Gaussian envelope of the optical lattice has a major influence on the properties of the reflector. In particular, it gives rise to multiple reflections of the wave packet between two symmetric locations where Bragg reflection occurs. Our results are a further step towards integrated atom-optics setups for quasi-cw matter waves.

DOI: 10.1103/PhysRevLett.107.230401 PACS numbers: 03.75.Kk, 03.75.Lm

The interaction of light with structures having a periodic refractive index profile is ubiquitous in photonics. Applications range from simple antireflection coatings to the fabrication of dielectric mirrors with ultrahigh reflectivities, used for instance in high-finesse cavities, and to semiconductor laser technology with the example of vertical cavity surface-emitting lasers (VCSELs), and distributed feedback or distributed Bragg reflector lasers. In the field of guided optics, fiber Bragg gratings are essential components for the telecommunication industry, as well as for the realization of outcoupling mirrors in high-power fiber lasers. Photonic crystal devices also have a huge range of applications [1].

In matter wave optics and interferometry, interactions of free-space propagating beams or trapped clouds with periodic structures or potentials have been extensively investigated and are commonly used as mirrors and beam splitters [2–4]. In this Letter, we demonstrate, following the proposals of Refs. [5–9], a Bragg reflector for manipulating a guided Bose-Einstein condensate (BEC) propagating in an optical waveguide, i.e., the exact atom-optics counterpart of a photonic fiber Bragg grating. We study the dynamics and the transmission of a probe wave packet as a function of the depth of the optical lattice. As we will develop later on, this quasi-1D configuration clearly exemplifies two textbook features of quantum mechanics: quantum reflection [10–12] and band theory [13,14]. This Letter is organized as follows. We first present a simple model to gain some physical insight into the Bragg reflection of a matter wave packet by a finite-length lattice having a Gaussian envelope. Then we describe our experimental implementation and show quantitative agreement between the data and our model. Finally, we discuss numerical simulations that give access to unresolved details in the experiment.

We consider a BEC with given mean velocity $\bar{v}$ and dispersion Δv propagating in a horizontal waveguide defining the x axis. At some distance, two intersecting laser beams interfere and create an *attractive* quasiperiodic potential of finite length, with lattice spacing d (see Fig. 1).

The potential experienced by the atoms is modeled by

$$U(x) = -U_0 \exp\left(-\frac{2x^2}{\tilde{w}^2}\right)\sin^2\left(\frac{\pi x}{d}\right), \tag{1}$$

whose depth $U_0 > 0$ is proportional to the power of the laser beams. The period d naturally introduces typical scales in velocity $v_R = h/(md)$ and energy $E_R = mv_R^2/2$.

We are interested in a wave packet with finite size and velocity dispersion impinging on a finite-length lattice. Let us consider first the textbook case of an incident plane wave and a square-envelope lattice (see, e.g., [15] for an analytical treatment of the problem). Figure 2(a) shows the transmission coefficient for a lattice of $N = 800$ sites, calculated by solving numerically the corresponding stationary Schrödinger equation. For a given velocity v, one observes that the transmission coefficient essentially

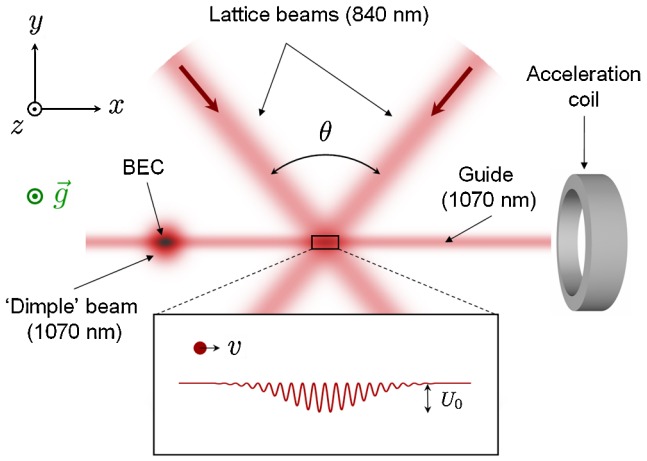

FIG. 1 (color online). Schematic view of the experimental setup (not to scale).

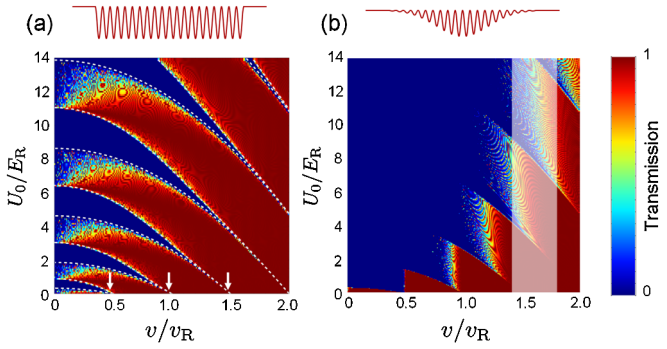

FIG. 2 (color online). Intensity transmission coefficient of the lattice for an incident plane wave of velocity v, as a function of the lattice depth U_0. (a) Square-envelope lattice with 800 sites. The white dashed lines are obtained from the Mathieu characteristic functions; white arrows show the velocities for which the Bragg condition is fulfilled (see text). (b) Lattice with a Gaussian envelope ($1/e^2$ radius $\tilde{w} \simeq 230d$). The vertical shaded stripe corresponds to the relevant velocity components in the wave packet used for the measurements shown in Figs. 3 and 4. The insets on top of (a) and (b) illustrate the shape of the lattice envelope, but the number of sites is reduced to $N = 20$ for clarity.

switches between 0 and 1 as a function of the depth of the lattice U_0. It can be interpreted as follows. At the entrance, the incoming state of energy $E_i = mv^2/2$ is projected onto the eigenstates of the lattice. The associated eigenenergies distribute into energy bands [13] whose position can be expressed in terms of the characteristic functions of the Mathieu equation [16,17] as depicted by the white dashed lines in Fig. 2(a). Reflection occurs if E_i lies in the gap between two allowed energy bands. Because of the finite length of the lattice the energy bands are not strictly continuous and resolve into N separate states for vanishing incident velocity [17]. Undersampling of the image gives rise to the "foamy" aspect of the low-velocity side of transmission bands. Obviously, the reflection by an *attractive* potential is a purely quantum effect, with no classical counterpart.

A second interesting feature appears in the limit of a vanishing potential depth U_0. One still observes reflection but it occurs only for incident velocities of the form $v = nv_R/2$ where n is an integer [see the white arrows in Fig. 2(a)]. This corresponds to Bragg's condition $2d\sin\Theta = n\lambda$ [14], where $\Theta = \pi/2$ for retroreflection, and $\lambda = h/(mv)$ is the incident de Broglie wavelength of the atoms: the reflection amplitude at each lattice site is small, but constructive interference between all the reflected waves results in a macroscopic reflected wave building up. For the range of parameters of Fig. 2(a), quantum reflection by a *single* lattice well occurs only for velocities that are very small as compared to v_R [17] and thus cannot explain the observed features.

Figure 2(b) shows the result of the same calculation, but now for the experimentally relevant case of a lattice having a smooth Gaussian envelope. One clearly observes a drastic change in the dependence of the transmission coefficient: for a fixed velocity v, the transmission is essentially equal to one only *below* a critical value $U_0^{(1)}$ of the lattice depth, and then goes essentially to zero for increasing U_0 (except for very narrow resonances). That critical value corresponds to the smallest one at which total reflection would occur for the square-envelope lattice. Almost no resurgence of the transmission is observed if U_0 is further increased, which gives a "sawtooth" appearance to the boundary between reflection and transmission.

This can be understood as follows. We are in the slowly varying envelope limit as $\tilde{w} \gg d$. The amplitude of the lattice does not change appreciably over a few sites, and thus one can consider that, locally, the matter wave interacts with a constant-amplitude lattice. When $U_0 = U_0^{(1)}$ the reflection condition is met at the center of the lattice, i.e., at $x = 0$. Then, for higher values of U_0, there are some locations $\pm x_{\mathrm{refl}}$, on both sides of the center, for which $U(\pm x_{\mathrm{refl}}) = U_0^{(1)}$. In this case, reflection occurs at $x = -x_{\mathrm{refl}}$. If there were not a second, identical mirror at $x = x_{\mathrm{refl}}$, the transmission of the lattice would strictly vanish for $U_0 > U_0^{(1)}$. However, as in optics, the two local Bragg mirrors actually constitute a Fabry-Perot resonator, analog to a VCSEL cavity for example, and transmission exhibits sharp resonances which gives the same foamy aspect as in Fig. 2(a).

We now come to the experimental realization. Our technique to produce all-optical BECs has been described in detail elsewhere [18]; in what follows we thus simply recall the major steps. We produce an almost pure ^{87}Rb condensate containing typically 5×10^4 atoms by forced evaporation over 4 s in a crossed optical dipole trap. It is made of two intersecting beams with a wavelength of 1070 nm. A horizontal one, with a waist of 50 μm, to be used later as a guide for the BEC, defines the $\hat{x}$ direction. The second, the "dimple" beam, of waist 150 μm, propagates along the diagonal in the (x, z) plane, $\hat{z}$ being the vertical (Fig. 1). Spin distillation using a magnetic field gradient during evaporation [18] results in the BEC being prepared in the state $|F = 1, m_F = 0\rangle$. We then decrease adiabatically the power in the dimple beam by a factor $\sim$20 over 80 ms, thus barely keeping a longitudinal confinement for the BEC, before switching it off abruptly to outcouple a wave packet in the horizontal guide. In this way, we produce a wave packet with a minimal intrinsic longitudinal velocity dispersion [19,20]. To set the wave packet in motion, we then switch on a coil, coaxial with the guide, that produces an inhomogeneous magnetic field. Through the quadratic Zeeman effect the wave packet is accelerated in 15 ms to a final mean velocity $\bar{v} = 11$ mm/s. The residual acceleration of the packet due to stray fields and beam curvature is negligible (we measure an upper bound of 10 mm/s^2).

Centered 350 μm downstream from the dimple location x_0, the optical lattice is produced at the intersection of two

beams with a wavelength $\lambda_L = 840$ nm (red-detuned with respect to the ^{87}Rb $D1$ and $D2$ lines) and a waist $w = 110$ μm, linearly polarized along $\hat{z}$, crossing at an angle $\theta \simeq 81°$. The lattice detuning is large enough so that spontaneous emission does not play any role in our experimental time scales. The resulting lattice spacing is $d = \lambda_L/[2\sin(\theta/2)] \simeq 650$ nm, and the envelope $1/e^2$ radius is $\tilde{w} = w/\cos(\theta/2) \simeq 145$ μm. In a set of preliminary experiments we calibrate the potential depth U_0 using Kapitza-Dirac (KD) diffraction [21,22]. A BEC is created at the position of the lattice and exposed to the lattice potential for a short time τ_{KD}, typically a few tens of microseconds. The diffraction pattern of the BEC after time of flight as a function of τ_{KD} is then compared to numerical simulations of the process. A typical 35 mW per beam results in U_0 up to $15E_R$.

After being launched as described above, the wave packet propagates in the horizontal guide for an adjustable time t_{prop}. Then all the lasers are switched off abruptly and the cloud is imaged by absorption after a 10 ms time of flight. This gives access to the spatial density distribution $n(x, t) = |\psi(x, t)|^2$ of the wave packet with a resolution of about 10 μm limited by the numerical aperture of our collection lens.

In a first set of experiments, the propagation time $t_{\mathrm{prop}} = 100$ ms is sufficiently long so that the interaction with the lattice is completed. We measured in a separate experiment the mean velocity $\bar{v} \simeq 11$ mm/s $\simeq 1.6v_R$ and a rms velocity spread $\Delta v \simeq 1.3$ mm/s $\simeq 0.2v_R$ corresponding to the shaded region of Fig. 2(b). For each lattice depth U_0, an average image is generated from eight individual runs and then integrated along the transverse direction $\hat{y}$. Figure 3(a) is a stack of 55 such profiles. For sake of comparison, Fig. 3(b) is the result of a numerical simulation of the wave packet dynamics using the one-dimensional Schrödinger equation solved by the split-Fourier method; the initial condition is a Gaussian wave packet with the experimentally measured momentum and position dispersions [19]. There is no adjustable parameter and the overall agreement with experimental data means that our simple 1D model captures most of the physics involved.

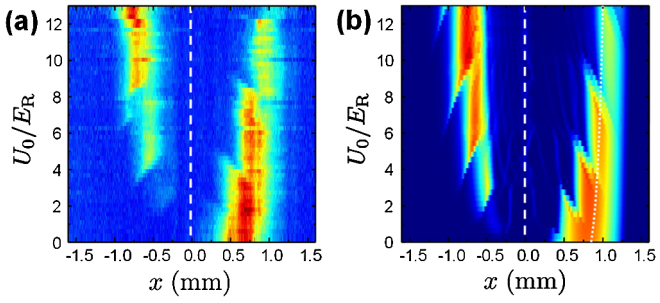

FIG. 3 (color online). (a) Measured density distribution of the wave packet (of initial mean velocity $\bar{v} = 11$ mm/s) after a propagation time $t_{\mathrm{prop}} = 100$ ms, for different lattice depths U_0. Each horizontal line is the average of typically eight absorption images integrated along the $\hat{y}$ direction. The vertical white dashed line shows the position of the center of the lattice. (b) Results of the simulation without any adjustable parameters. The finite resolution of the imaging system (~ 10 μm) is included. The dotted line is the expected position of the center of the wave packet according to classical dynamics (see text).

Let us concentrate first on the transmitted part of the wave packet ($x > 0$). If there were no lattice, the propagation time t_{prop} is long enough so that the initial size of the wave packet is negligible with respect to its size after propagation. The spatial distribution of the wave packet would then be a direct mapping of its initial velocity distribution $f(v)$: $n(x, t_{\mathrm{prop}}) \propto f[(x - x_0)/t_{\mathrm{prop}}]$.

One can then understand intuitively the main features of Fig. 3 for the scattering of a wave packet, from the transmission coefficients shown in Fig. 2(b) for a plane wave. In the background of the shaded area of Fig. 2(b) representing the wave packet one can see the transmitted and reflected components. In the presence of the lattice, the reflected part propagates backwards and is located, for the propagation time chosen here, at a symmetrical position. This explains why the transmitted and reflected wave packets appear like a complementary mirrored image of each other. The sawtoothlike boundary, reminiscent of the transmission diagram, is a fingerprint of the band structure inside the lattice. However, the effect of the lattice potential is not limited to the one of the sinusoidal component, responsible for the Bragg reflection described above. The spatially averaged attractive potential also accelerates the wave packet. The white dotted line in Fig. 3(b) shows the final position of a classical particle starting with velocity $\bar{v}$ from position x_0 and propagating for a time t_{prop}, taking into account its acceleration by the spatially averaged lattice potential. The fair agreement with the data indicates that the slight curvature in the position of the wave packet as a function of U_0 simply arises from this classical effect.

Beyond studying the asymptotic scattering states, it is also possible to visualize the dynamics of the interaction by varying t_{prop}. Figure 4(a) displays such a time sequence that fairly compares to the numerical simulation depicted in the same conditions in Fig. 4(b). One clearly observes the spreading of the incident wave packet over the whole lattice for $30 \lesssim t_{\mathrm{prop}} \lesssim 45$ ms and its subsequent splitting into a reflected and a transmitted one. Unfortunately, the details of the inner dynamics are washed out by the free expansion of the wave packet during the time-of-flight sequence and the finite resolution of the imaging system.

Numerical simulations, properly checked against the previous experimental results, are useful here. In Fig. 4(c) we have deliberately suppressed the time-of-flight period and enhanced the optical resolution and the contrast with respect to Fig. 4(b): one then clearly observes multiple reflections of some components of the wave packet at symmetric positions $\pm x_{\mathrm{refl}}$, with decreasing amplitude at

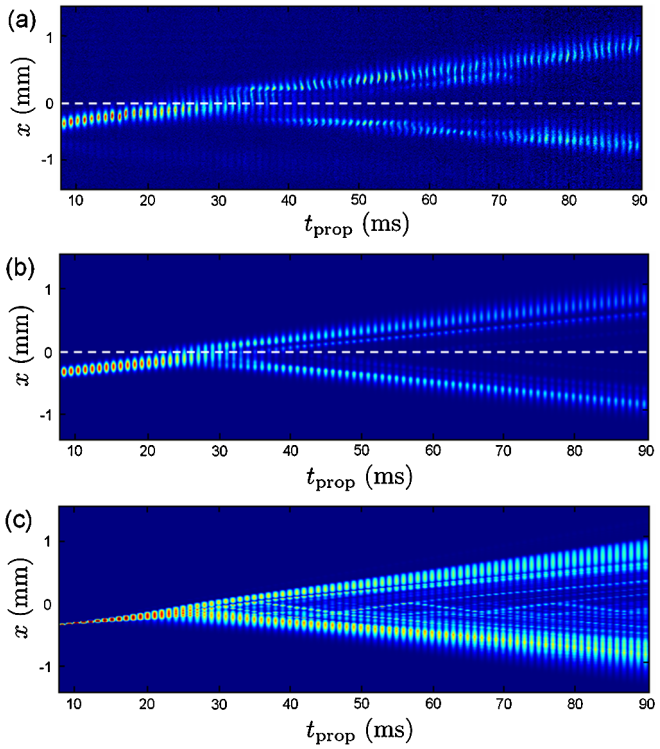

FIG. 4 (color online). Time sequence showing the scattering of a wave packet with mean velocity $\bar{v} \simeq 11$ mm/s on the optical lattice for $U_0 \simeq 11E_R$. The white dashed lines in (a) and (b) show the position of the center of the lattice. The time interval between successive images is 1 ms. (a) Experimental data. (b) Simulation, taking into account the finite imaging resolution as well as the time of flight (TOF) period. (c) Same as (b) but without TOF nor reduced resolution; the color scale is nonlinear in order to enhance contrast.

each bounce. This "cavity-ring-down" behavior explains the formation of structures in the transmitted and reflected wave packets as observed in Fig. 4(a) and especially visible as a parallel lower stripe in the transmitted wave packet for $50 \lesssim t_{\mathrm{prop}} \lesssim 75$ ms. However, experimentally, observing several bounces is not possible here due to the small number of atoms involved.

In the same way, in images such as Fig. 3 the reflected wave packet appears to be relatively smooth. It is actually not the case, as can be seen in simulations with full resolution (Fig. 5). The lattice acts as a matter wave interference filter with very narrow features due to the high number of lattice sites (foamy zones of Fig. 2).

Until now we have used a simple one-dimensional description of the system. However, the system is actually far from being one dimensional, since the transverse quantum of energy $\hbar\omega_\perp \simeq h \times 90$ Hz is much smaller than the typical longitudinal energy scales, typically by 2 orders of magnitude. Our simple one-dimensional model agrees well with the experimental results as shown above because couplings between longitudinal and transverse degrees of freedom are weak (they are due only to experimental

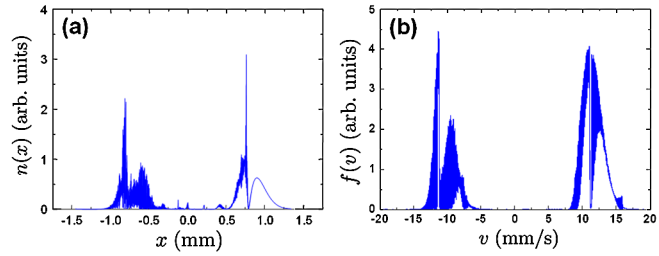

FIG. 5 (color online). (a) Calculated density and (b) velocity distribution of a wave packet of initial mean velocity $\bar{v} = 11$ mm/s after a propagation time $t_{\mathrm{prop}} = 100$ ms with full resolution. The lattice depth is $U_0 = 8E_R$.

imperfections such as misalignments of the lattice beams with respect to the guide, for instance); some transverse excitations can nevertheless be observed on our data [see, e.g., the long wavelength dipole oscillations in Fig. 4(a), especially for $t_{\mathrm{prop}} \gtrsim 30$ ms]. Stronger couplings would be expected to significantly alter the scattering properties of the structure [23,24].

In conclusion, we have studied in detail the scattering of a guided matter wave by a finite-length optical lattice in the slowly varying envelope limit. The experiments can be interpreted in the framework of a local band structure, and the whole lattice can be seen as a cavity based on Bragg mirrors.

Major improvements are expected with the use of high numerical aperture optics [25,26]. Drastically reducing the length $\tilde{w}$ of the lattice and thus generating a structure consisting of only a few sites, possibly with a shaped envelope, one could tailor almost arbitrarily the matter wave filter response. The latter can also be altered using a moving optical lattice [27,28]. The transmission band of the filter could then be adjusted at will. Such setups would prove useful in measuring, for instance, the coherence length [29] of guided atom lasers [30–32]. In a different direction, it would be appealing to study the effect of interatomic interactions [33] on the propagation of the wave packet, with the possible appearance of soliton trains [34] or atom-blockade effects [35]. This regime could be reached by using much higher transverse frequencies for the guide, in order to enhance the effects of nonlinearities.

We thank I. Carusotto for useful discussions, and acknowledge support from Agence Nationale de la Recherche (GALOP project), Région Midi-Pyrénées, and Institut Universitaire de France.

[1] B. E. A. Saleh and M. C. Teich, *Fundamentals of Photonics* (Wiley InterScience, New York, 2007).
[2] A. D. Cronin, J. Schmiedmayer, and D. E. Pritchard, Rev. Mod. Phys. **81**, 1051 (2009).
[3] D. E. Pritchard *et al.*, Ann. Phys. (Leipzig) **10**, 35 (2001).
[4] S. L. Rolston and W. D. Phillips, Nature (London) **416**, 219 (2002).

[5] L. Santos and L. Roso, J. Phys. B **30**, 5169 (1997).
[6] L. Santos and L. Roso, Phys. Rev. A **58**, 2407 (1998).
[7] N. Friedman, R. Ozeri, and N. Davidson, J. Opt. Soc. Am. B **15**, 1749 (1998).
[8] I. Carusotto, M. Artoni, and G. C. La Rocca, Phys. Rev. A **62**, 063606 (2000).
[9] T. Lauber *et al.*, J. Phys. B **44**, 065301 (2011).
[10] C. Cohen-Tannoudji, B. Diu, and F. Laloë, *Quantum Mechanics* (Wiley, New York, 1977).
[11] F. Shimizu, Phys. Rev. Lett. **86**, 987 (2001).
[12] T. A. Pasquini *et al.*, Phys. Rev. Lett. **93**, 223201 (2004).
[13] C. Kittel, *Introduction to Solid-State Physics* (Wiley, New York, 1953).
[14] N. W. Ashcroft and N. D. Mermin, *Solid State Physics* (Saunders, Philadelphia, PA, 1976).
[15] D. W. L. Sprung, H. Wu, and J. Martorell, Am. J. Phys. **61**, 1118 (1993).
[16] N. W. McLachlan, *Theory and Application of Mathieu Functions* (Oxford University Press, Oxford, 1947).
[17] See Supplemental Material at http://link.aps.org/supplemental/10.1103/PhysRevLett.107.230401 for more details.
[18] A. Couvert *et al.*, Europhys. Lett. **83**, 50001 (2008).
[19] Nonlinearities due to atom-atom interactions are negligible for the dilute wave packets studied here, and thus are not accounted for in the simulation (the chemical potential of the BEC when it reaches the lattice is on the order of $0.1E_R$, and thus negligible as compared to any longitudinal energy scale). The only effect of interactions is to set (in addition to the quantum pressure) the velocity dispersion of the wave packet in the initial stages of the expansion in the guide, by conversion of the interaction energy of the BEC into kinetic energy. For more details, see [20].
[20] F. Vermersch *et al.*, Phys. Rev. A **84**, 043618 (2011).
[21] B. Gadway *et al.*, Opt. Express **17**, 19173 (2009).
[22] J. H. Huckans *et al.*, Phys. Rev. A **80**, 043609 (2009).
[23] G. L. Gattobigio, A. Couvert, B. Georgeot, and D. Guéry-Odelin, New J. Phys. **12**, 085013 (2010).
[24] G. L. Gattobigio, A. Couvert, B. Georgeot, and D. Guéry-Odelin, arXiv:1105.1971.
[25] Y. R. P. Sortais *et al.*, Phys. Rev. A **75**, 013406 (2007).
[26] K. Henderson *et al.*, New J. Phys. **11**, 043030 (2009).
[27] L. Fallani *et al.*, Phys. Rev. Lett. **91**, 240405 (2003).
[28] B. Eiermann *et al.*, Phys. Rev. Lett. **91**, 060402 (2003).
[29] M. Köhl, T. W. Hänsch, and T. Esslinger, Phys. Rev. Lett. **87**, 160404 (2001).
[30] W. Guérin *et al.*, Phys. Rev. Lett. **97**, 200402 (2006).
[31] J. Billy *et al.*, Ann. Phys. (Paris) **32**, 17 (2007).
[32] A. Bernard *et al.*, New J. Phys. **13**, 065015 (2011).
[33] O. Morsch and M. K. Oberthaler, Rev. Mod. Phys. **78**, 179 (2006).
[34] I. Carusotto, D. Embriaco, and G. C. La Rocca, Phys. Rev. A **65**, 053611 (2002).
[35] I. Carusotto, Phys. Rev. A **63**, 023610 (2001).